Radiation of optical angular momentum from a dipole source in a magneto-birefringent disordered environment

R. Le Fournis and B. A. van Tiggelen*
Universite Grenoble Alpes, CNRS, LPMMC, 38000 Grenoble, France

(Received 17 July 2023; accepted 16 October 2023; published 15 November 2023)

We investigate the radiation of optical angular momentum by a dipole gas under uniform magnetic field with an unpolarized source at its center. Conservation of angular momentum implies a torque on both the source and the surrounding environment. We study the separate spin and orbital contributions to the radiated angular momentum.

DOI: 10.1103/PhysRevA.108.053713

I. INTRODUCTION: TORQUES AND SOURCES

Radiative forces have been studied since Maxwell's equations have appeared more than 150 years ago. Radiative pressure due to light scattering is a major force after gravity in astrophysics [1]. Today, radiative forces are widely used to manipulate matter and cool atoms with optical traps and optical tweezers. Even in the quantum vacuum, new radiative forces emerge, such as the Casimir force [2] and quantum vacuum friction [3,4]. They fascinate theoreticians, and after all these years some controversies still exist in the definition of photon momentum [5]. Of course, it is well known that light possesses angular momentum and can transfer angular momentum when interacting with matter. By conservation of angular momentum, any emitter of electromagnetic angular momentum must suffer from a mechanical back reaction. Magnetized neutron stars radiate electromagnetic angular momentum and their rotation is slowed down [6].

The classical or quantum emission of electromagnetic waves is an active field of research. Today it widely acknowledged that the radiative power of a source is not only determined by its internal structure of moving charges and currents but also by its direct environment [7]. The emission of radiation from a dipole source, such as an atom or a quantum emitter, can be significantly affected by its environment. An important phenomenon in this context is the Purcell effect [8]. It refers to the modification of the radiative properties of a source when placed in close proximity to an environment with specific optical properties. This property must also apply to sources of optical angular momentum. Well-known emitters of electromagnetic angular momentum are rotating charges or magnetic moments, including atoms in quantum states with high angular momentum. The amount of radiated angular momentum should depend on the environment and vice versa, both emitter and environment must be subject to a torque.

The main motivation of this work is to study an ultimate situation where a classical electric dipole—a source for radiation of energy but not of angular momentum [9]—becomes an emitter of angular momentum due to a magneto-birefringent environment. We will investigate the back reaction to both environment and source. The radiated angular momentum is expected to contain both spin and orbital motion. This reveals that the action and dynamics of source, local environment, and emitted radiation are intimately connected. In our first study [10] we considered the emission of electromagnetic angular momentum and did not address the back reaction of the scatterers in detail. In our previous study [11] we dealt with a homogeneous, spherical environment in which the environment was seen not to be subject to a torque but only the source. In our present model the environment is disordered and both source and environment experience a torque due to light scattering.

II. RADIATION OF OPTICAL ANGULAR MOMENTUM

We consider an unpolarized dipole source in the center of a spherical environment with radius R containing a gas of N pointlike electric dipoles (Fig. 1). The electric dipoles have polarizability [12]:

$$\boldsymbol{\alpha}(\omega, \boldsymbol{B}_0) = \frac{\alpha(0)\omega_0^2}{\omega_0^2 - (\omega + \omega_c i\boldsymbol{\epsilon}\cdot\hat{\boldsymbol{B}}_0)^2 - i\gamma\omega}, \tag{1}$$

where γ is the radiative damping rate of the dipoles, ω_0 is the resonance frequency and $\omega_c = eB_0/2mc_0$ is the cyclotron frequency; and $\alpha(0)$ is the static polarizability and can be related to the volume u of the dipoles as $\alpha(0) = 3u$ [13]. The hermitian 3×3 matrix $i(\boldsymbol{\epsilon}\cdot\hat{\boldsymbol{B}}_0)_{nm}$ is defined as $i\epsilon_{nmk}\hat{B}_{0k}$. In a microscopic theory, $\hbar\omega_c$ represents the Zeeman splitting of an excited state due to the interaction of the atom with the magnetic field. The continuity equation for the angular momentum $\boldsymbol{J}(r,t)$ confined in a sphere of radius r at time t around the source is given by [9]

$$\frac{d}{dt}\left[J_k^{\text{mech}} + J_k^{\text{rad}}\right](r,t) = \frac{r^3}{8\pi}\epsilon_{klm}\text{Re}\int d\hat{\boldsymbol{r}}'\,\hat{r}'_j\hat{r}'_l(E_j\bar{E}_m + B_j\bar{B}_m)(r\hat{\boldsymbol{r}}',t)$$

$$\frac{d}{dt}J_k^{\text{mech}} \equiv \mathbf{M}_{\mathbf{k}}. \tag{2}$$

*Bart.Van-Tiggelen@lpmmc.cnrs.fr

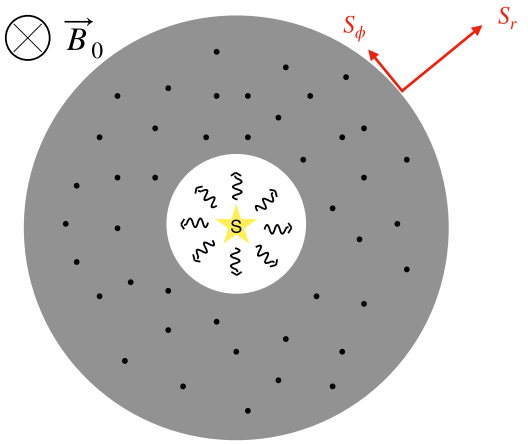

FIG. 1. Schematic picture of the geometry considered in this work. An unpolarized dipole source is located at the origin, surrounded by two shells: the first shell is empty to avoid scattering close to the source, while the second shell contains an on average homogeneous dipole gas with radius R. The external magnetic field is directed perpendicular to the plane. The electromagnetic Poynting vector exhibits an azimuthal component $\boldsymbol{S}_\phi$ which is orthogonal to both the magnetic field and the radial vector. This component induces the emission of angular momentum into space.

The right-hand side of this equation represents the optical angular momentum (AM) radiated into space. Summation over repeated vector indices j, l, m has been assumed implicitly. For $r > R$ the mechanical AM is independent of distance r, and $d\boldsymbol{J}^{\text{mech}}/dt$ gives the torque on both source and environment. If the source has been stationary for a time much longer than it takes light to travel a distance equal to the radius r ($t \gg r/c_0$), the total electromagnetic AM inside the sphere of radius r stays constant, so that $d\boldsymbol{J}^{\text{rad}}(r,t)/dt = \boldsymbol{0}$. In that case the leakage is independent on the distance r. According to Eq. (2), matter experiences a torque equal to the emitted AM. To determine the amount of AM emitted, we can evaluate the right-hand side of Eq. (2) at a large distance from the environment ($r \to \infty$). The electric and magnetic fields in Eq. (2) are determined by solving the Helmholtz equation for a classical monochromatic source with frequency $\omega = kc_0$ [14]. The solutions for the electric and magnetic fields can be expressed as

$$\begin{aligned}\boldsymbol{E}(\boldsymbol{r}) &= \boldsymbol{G}^E(\boldsymbol{r}) \cdot \big(-4\pi i\omega/c_0^2\big)\boldsymbol{j}_S,\\ \boldsymbol{B}(\boldsymbol{r}) &= \boldsymbol{G}^B(\boldsymbol{r}) \cdot \big(-4\pi i\omega/c_0^2\big)\boldsymbol{j}_S.\end{aligned} \tag{3}$$

We define the Green's functions as $\boldsymbol{G}^E(\boldsymbol{R})$ and $\boldsymbol{G}^B(\boldsymbol{R})$ according to

$$\boldsymbol{G}^E(\boldsymbol{r}) = \boldsymbol{G}^0(\boldsymbol{r}) + \sum_{\alpha,\beta} \boldsymbol{G}^0(\boldsymbol{r}-\boldsymbol{R}_\alpha)\cdot\boldsymbol{T}_{\alpha\beta}\cdot\boldsymbol{G}^0(\boldsymbol{R}_\beta), \tag{4}$$

$$\boldsymbol{G}^B(\boldsymbol{r}) = \boldsymbol{G}_B^0(\boldsymbol{r}) + \sum_{\alpha,\beta} \boldsymbol{G}_B^0(\boldsymbol{r}-\boldsymbol{R}_\alpha)\cdot\boldsymbol{T}_{\alpha\beta}\cdot\boldsymbol{G}^0(\boldsymbol{R}_\beta). \tag{5}$$

To distinguish between the spatial components and the dipole indices of the tensors, we use Latin and Greek indices, respectively. The dot denotes the contraction of Latin indices associated with polarization. The Green's functions $\boldsymbol{G}^0$ and $\boldsymbol{G}_B^0$ describe how the electromagnetic waves generated by the electric dipole source propagate in free space and can be obtained from [15]. For a monochromatic electric dipole source at the origin with a dipole moment $\boldsymbol{d}$, the source current is $\boldsymbol{j}_S(\boldsymbol{r}) = -i\omega\boldsymbol{d}\delta(\boldsymbol{r})$. The transmission matrix $\boldsymbol{T}_{\alpha\beta}$, that appears in both Green's functions, is a $3N\times 3N$ matrix. It describes how light emanating from a source and interacting with a gas of electric dipoles propagates through the environment. The factor 3 corresponds to the three polarization states of light. The T matrix can be calculated as described in [13]. We will first put $\boldsymbol{B}_0 = \boldsymbol{0}$ and treat the external magnetic field later in perturbation. Without an external magnetic field, the T matrix is given by

$$\big\{\boldsymbol{T}^{(0)}_{\alpha\beta}\big\} = \frac{t_0(\omega)}{\{\boldsymbol{1}\delta_{\alpha\beta} - t_0(\omega)\boldsymbol{G}^0(\boldsymbol{R}_\alpha - \boldsymbol{R}_\beta)(1-\delta_{\alpha\beta})\}}. \tag{6}$$

The superscript (0) indicates that this is the T matrix in the absence of an external magnetic field; $t_0(\omega)$ is the T matrix of a single electric dipole and is expressed near its resonance frequency $\omega_0 = c_0k_0$ as

$$\boldsymbol{t}_0(\omega) = -\boldsymbol{\alpha}(\omega, \boldsymbol{B}_0 = \boldsymbol{0})k^2 = \frac{3\pi}{k_0}\frac{1}{\delta + i/2}\boldsymbol{1}. \tag{7}$$

We introduced the detuning parameter δ [13], which is the difference between the frequency ω of the source and the resonance frequency ω_0 of the surrounding dipoles divided by the decay rate of the dipoles. The frequency ω is assumed to be near the resonance and $\gamma \ll \omega_0$, so that we set $k = k_0$ in the Green's tensor. The T matrix describes a nonabsorbing medium, and in our numerical implementation we explicitly verified the optical theorem. The presence of an external magnetic field in the polarizability (1) modifies the T matrix [16]. The change is small and can be treated perturbatively. In first order, the modified T matrix is given by

$$\boldsymbol{T}_{\alpha\beta} = \boldsymbol{T}^{(0)}_{\alpha\beta} + \boldsymbol{T}^{(0)}_{\alpha\gamma}\cdot\left[\delta_{\gamma\delta}\left(-i\frac{k_0}{6\pi}\mu\boldsymbol{\epsilon}\cdot\hat{\boldsymbol{B}}_0\right)\right]\cdot\boldsymbol{T}^{(0)}_{\delta\beta}. \tag{8}$$

The dimensionless parameter μ is deduced from the expression of the polarizability (1) in the presence of the magnetic field:

$$\mu = \frac{12\pi}{\alpha(0)k_0^3}\frac{\omega_c}{\omega_0}. \tag{9}$$

All torques calculated in this paper will be linearly proportional to μ, itself linear in the external magnetic field. In this diamagnetic picture, $\mu \sim 5\times10^{-5}$/Gauss is small (calculated, e.g., for a hydrogen atom and the transition $1S \to 2P$). The material parameter μ is the small parameter in our perturbation expansion. Its smallness guarantees that for any realistic magnetic field, up to Tesla's, the linear perturbation is valid.

The mechanical torque in Eq. (2) can be split into two parts: the torque on the source $\boldsymbol{M}^{\text{S}}$ and the torque on the environment. The torque on the source is given by [11]

$$M_i^{\text{S}} = -\frac{2\pi}{3}k^2|\boldsymbol{d}|^2\,\text{Re}\,\epsilon_{ijk}G^E_{kj}(\boldsymbol{0},\boldsymbol{0}). \tag{10}$$

By conservation of AM, the torque on the environment equals the difference between the torque on the source and the AM leakage $\boldsymbol{M}^{\text{E}} = \boldsymbol{M} - \boldsymbol{M}^{\text{S}}$.

III. COMPUTATION OF THE RADIATED OPTICAL ANGULAR MOMENTUM

The right-hand side of Eq. (2) represents the radiation of optical AM as mentioned, which includes a front factor proportional to r^3. This factor means that the AM emitted at infinity can be found by keeping only those terms in $\bar{E}_l E_k$ and $\bar{B}_l B_k$ that are proportional to $1/r^3$ and that the leading terms $1/r^2$ vanish. We assume an unpolarized source, facilitated by a random orientation of the dipole vector $\boldsymbol{d}$ of the source. The tensor $\bar{E}_j E_m$ for an unpolarized source is expressed as

$$\begin{aligned}\bar{E}_j(\boldsymbol{r})E_m(\boldsymbol{r}) = \frac{(4\pi)^2}{3}k_0^4|\boldsymbol{d}|^2\Big[& G^0_{js}(\boldsymbol{r})\bar{G}^0_{ms}(\boldsymbol{r}) \\ & + \sum_{\alpha,\beta} G^0_{js}(\boldsymbol{r})\bar{G}^0_{mn}(\boldsymbol{r}-\boldsymbol{R}_\alpha)(\bar{T}_{\alpha\beta})_{nn'}\bar{G}^0_{n's}(\boldsymbol{R}_\beta) \\ & + \sum_{\alpha,\beta} G^0_{jn}(\boldsymbol{r}-\boldsymbol{R}_\alpha)(T_{\alpha\beta})_{nn'}G^0_{n's}(\boldsymbol{R}_\beta)\bar{G}^0_{ms}(\boldsymbol{r}) \\ & + \sum_{\alpha,\beta,\gamma,\delta} G^0_{jn}(\boldsymbol{r}-\boldsymbol{R}_\alpha)(T_{\alpha\beta})_{nn'}G^0_{n's}(\boldsymbol{R}_\beta) \\ & \times \bar{G}^0_{mp}(\boldsymbol{r}-\boldsymbol{R}_\gamma)(\bar{T}_{\gamma\delta})_{pp'}\bar{G}^0_{p's}(\boldsymbol{R}_\delta)\Big]. \end{aligned} \tag{11}$$

A similar expression for the average tensor $\bar{B}_j B_m$ is obtained by the same procedure. The first term of Eq. (11) corresponds to the unscattered radiation of the source and does not contribute to the radiated AM. The second and third terms include the interference of the unscattered electric field emitted by the source and the electric field scattered by the dipole gas. The last term accounts for the interference among all multiple scattering paths inside the dipole gas. When considering the radiated optical AM at infinity, the angular integral in Eq. (2) simplifies and can be performed analytically. The general form of the expression for the radiated AM linear in the magnetic field is given by

$$M_k = X_k(\boldsymbol{R}_1,\ldots,\boldsymbol{R}_N) + A_{km}(\boldsymbol{R}_1,\ldots,\boldsymbol{R}_N)\hat{B}_{0,m}. \tag{12}$$

The vector $\boldsymbol{X}$ vanishes when only one dipole is considered but not for an arbitrary rotationally variant environment. The second term in Eq. (12) represents the torque linear in the magnetic field. We restore rotational invariance by averaging over the orientation of the dipole gas as a whole. This means that we rotate all position vectors of the scatterers by the same angle and then calculate the average over all possible rotations. The average of $\langle \boldsymbol{M}\cdot\hat{\boldsymbol{B}}_0\rangle$ over the dipole gas distribution orientation is physically equivalent to average over the direction of the magnetic field $\hat{\boldsymbol{B}}_0$:

$$\langle \boldsymbol{M}\cdot\hat{\boldsymbol{B}}_0\rangle = \langle \boldsymbol{M}\cdot\hat{\boldsymbol{B}}_0\rangle_{\hat{\boldsymbol{B}}_0}. \tag{13}$$

Averaging over the orientation of the dipole gas restores rotational symmetry. Consequently, only the direction of the external magnetic field remains for the radiated AM; this can be expressed as

$$\langle \boldsymbol{M}\rangle = \kappa_{\mathrm{L}}(\boldsymbol{R}_1,\ldots,\boldsymbol{R}_N)\hat{\boldsymbol{B}}_0. \tag{14}$$

The real-valued scalar κ_{L} refers to total leakage and is easily related to the second-rank tensor $\boldsymbol{A}$ using Eqs. (13) and (12):

$$\kappa_{\mathrm{L}} = \tfrac{1}{3}\mathrm{Tr}\boldsymbol{A}. \tag{15}$$

The same averaging of Eq. (10) leads to

$$\langle \boldsymbol{M}^{\mathrm{S}}\rangle = \kappa_{\mathrm{S}}\hat{\boldsymbol{B}}_0. \tag{16}$$

The calculation of κ_L for one single dipole, whose position is averaged over the same shell, has been done analytically. We used the analytical expression to calculate κ_L in the single scattering approximation (see Sec. V). After the average performed in Eqs. (15) and (16), κ_{L} and κ_{S} still fluctuate significantly with the exact choice for the N dipole positions. The full probability distributions functions, obtained for 1000 different sets of dipole positions, will be obtained later.

IV. ORBITAL AND SPIN ANGULAR MOMENTUM

In this section we separate the optical radiated AM into optical spin and orbital AM, and associate the total torque with the magneto-transverse component $\boldsymbol{S}_\phi$ of the Poynting vector in the far field. To obtain the latter we assume that the radiative AM propagates with the speed c_0 from the source and locate our outer surface at distance $r > c_0 t$ in Eq. (2) outside the light cone. The leakage through this surface now vanishes, and the total radiative angular moment for $r' < r$ evolves like

$$\frac{d\boldsymbol{J}^{\mathrm{rad}}}{dt} = \frac{d}{dt}\Big[\int_0^{c_0 t} dr'\, r'^2 \int d\hat{\boldsymbol{r}}'\,\boldsymbol{r}'\times\frac{\boldsymbol{S}(\boldsymbol{r}')}{c_0^2}\Big] = -\boldsymbol{M}, \tag{17}$$

where $\boldsymbol{S}(\boldsymbol{r})$ is the Poynting vector. This equation shows that $4\pi r'^3\langle\hat{\boldsymbol{r}}'\times\boldsymbol{S}_\phi\rangle_{\hat{\boldsymbol{r}}'}/c_0$ for $r' = c_0 t$ is equal to $-\boldsymbol{M}$. Hence, after averaging over the orientation of the dipole gas distribution, we get the simple expression

$$\int d\hat{\boldsymbol{r}}\,\hat{\boldsymbol{r}}\times\langle\boldsymbol{S}_\phi\rangle(\boldsymbol{r}) = -\frac{\kappa_{\mathrm{L}}c_0}{r^3}\hat{\boldsymbol{B}}_0. \tag{18}$$

In this approach we can separate the radiated AM into spin and orbital AM using [17]

$$\begin{aligned}\boldsymbol{M} &= \frac{r^2}{8\pi\omega}\mathrm{Im}\int d\hat{\boldsymbol{r}}\,[\boldsymbol{E}\times\bar{\boldsymbol{E}} + E_m(\boldsymbol{r}\times\boldsymbol{\nabla})\bar{E}_m] \\ &= \boldsymbol{M}^{\mathrm{spin}} + \boldsymbol{M}^{\mathrm{orbit}}. \end{aligned} \tag{19}$$

The angular integral in Eq. (19) must be evaluated on an arbitrary surface outside the environment. We evaluate it at infinity ($r\to\infty$), which allows us to perform the angular integral analytically. When evaluating the surface integral at infinity, only terms in the integrand that are proportional to $1/r^2$ need to be considered.

In conclusion, the scalar κ_{L} associated with total leakage of AM is related to an azimuthal Poynting vector that decays as $1/r^3$ and can be separated either into spin and orbital components or into torques exerted on environment and source:

$$\kappa_{\mathrm{L}} = \kappa_{\mathrm{Sp}} + \kappa_{\mathrm{O}} = \kappa_{\mathrm{S}} + \kappa_{\mathrm{E}}. \tag{20}$$

V. NUMERICAL RESULTS

In the numerical simulations, we calculate the dimensionless ratios $\kappa\omega/P_{\mathrm{S}}\mu$. Here P_{S} is the power emitted by the dipole source, which is also affected by the surrounding environment (Purcell effect [8]); κ refers to either κ_{L}, κ_{Sp}, etc. This ratio normalizes the torque to the amount of radiated energy and

quantifies the amount of emitted AM in units of $\hbar$ per emitted photon. The power emitted by the source is given by [11]

$$P_S = -\frac{2\pi}{3} k_0^3 c_0 |\boldsymbol{d}|^2 \mathrm{Im} G^E_{ii}(\mathbf{0}, \mathbf{0}). \tag{21}$$

The different ratios $\kappa\omega/P_S\mu$ are computed as a function of two parameters η and τ_0 defined as

$$\eta = \frac{4\pi n}{k_0^3}, \quad \tau_0 = \frac{R}{\ell_0} = Rn\sigma_{sc}. \tag{22}$$

The parameter η is the number of dipoles per cubic of wavelength, and τ_0 is (assuming independent scattering) the optical thickness, which is the ratio of the radius R of the sphere and the mean free path $\ell_0 = (n\sigma_{sc})^{-1}$; n is the scatterer density and σ_{sc} is the scattering cross section for one dipole. For $\eta \ll 1$, the contribution of recurrent scattering and interference to multiple scattering is expected to be negligible, but as η approaches unity, recurrent scattering can no longer be neglected. The neglect of recurrent scattering and interference is referred to as the independent scattering approximation (ISA) [18], so that ℓ_0 is the mean free path in the independent scattering approximation. For $\eta \sim 1$, the mean free path is usually larger than ℓ_0 [13]. We will ignore this change of the mean free path in the optical thickness τ_0 and use ℓ_0 to calculate the optical thickness.

The calculation time of our code increases rapidly as N^3 with the number of dipoles N. Apart from detuning, we have three dimensionless parameters that characterize our medium: η and τ defined in Eq. (22), and the size parameter of the sphere $x = kR$. Around resonance ($\delta \approx 0$) it can be seen that $\tau \sim N/x^2$ and $\eta \sim N/x^3$ so that $\eta \sim \tau/x$. Ideally we would like to have a medium with large multiple scattering and small recurrent scattering to avoid unknown complications, i.e., $\eta \ll 1$ and $\tau \gg 1$. This requires a large x and an even larger value for N. Because we are restricted to $N \leqslant 2000$, curves shown in the different figures stop at different values for τ. In the present study this prevented us from investigating $\tau > 6$ and $\eta < 0.03$. The last value still largely exceeds densities of scatterers in real-life environments.

In our numerical simulations we have excluded a small spherical region with a radius of $\lambda/4$ around the dipole source to avoid divergences due to the singular behavior of the Green's function at small $\boldsymbol{r}$ (see Fig. 1). We accounted for this small exclusion volume to obtain the value of τ_0 and η. However, we did not impose any constraints on the distance between the dipoles that would induce spatial correlations. We did not encounter any problems due to close dipoles in the simulations. To ensure the reliability of our results, we carefully ensured that the medium was on average homogeneous. We performed the full statistics of the value of the various kappas over at least 10^3 independent realizations for each data point, to be discussed later in Fig. 6.

We now present the numerical results. Figure 2 shows that for $\eta = 0.03$ the radiated AM is proportional to τ_0^2 and is directed opposite to the external magnetic field. This behavior is also expected to hold for smaller values of η that are more difficult to access numerically. For larger η, however, the τ_0^2 scaling disappears as τ_0 increases, and the radiated AM decreases as η increases at constant optical thickness. This figure illustrates the influence of recurrent scattering and

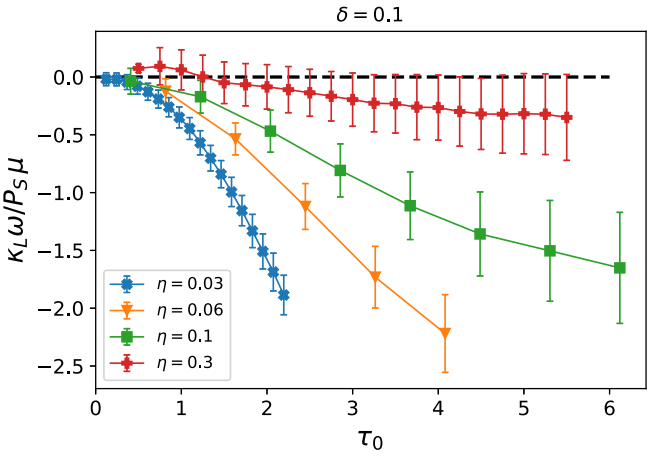

FIG. 2. Numerical results for the total leakage $\kappa_L\omega/P_S\mu$ per emitted photon for different values of the parameters η and τ_0. The bars indicate the standard deviation of the full statistic of κ_L values and are not error bars. The dashed line denotes the level zero.

interference on the radiated AM. More optical thickness increases the amount of radiated optical AM per photon, but larger values for η reduce the amount of radiated AM. The small leak of AM for large η may imply that interference phenomena suppress the propagation of AM inside the sphere. The result obtained for $\eta = 0.3$ and $\tau_0 \sim 1.25$ is quite remarkable, since the leak of AM actually vanishes, although the torque on the source still has a significant value (Fig. 4). This indicates that a direct transfer of AM exists from the source to the environment. For these parameters, the radiated spin and orbital AM are exactly opposite $\kappa_{Sp} + \kappa_O = 0$, with no net leak.

In Fig. 3 we show the numerical results for the spin component of the radiated AM. Surprisingly, we can see that the spin component represents only a small part of the total radiated AM, showing that the radiated AM is dominated by orbital AM. Only for $\eta = 0.3$, the spin part of total AM becomes significant.

In Fig. 4 we have plotted the torque acting on the source, given by the formula (10). It is strictly positive in the applied

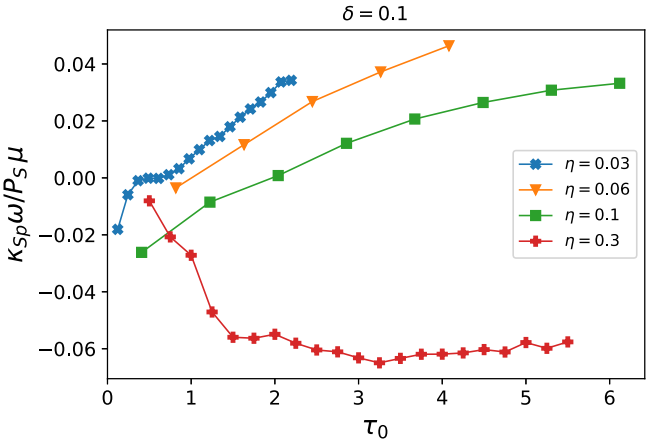

FIG. 3. Results of numerical simulations for the spin leakage $\kappa_{Sp}\omega/P_S\mu$ per emitted photon as a function of the optical thickness for various values of the parameter η.

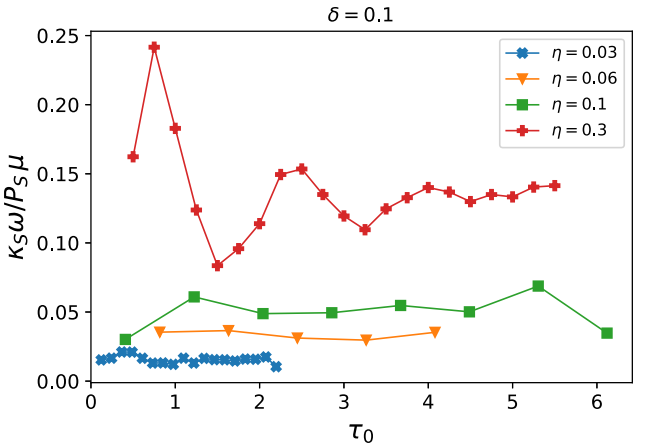

FIG. 4. Numerical results showing the torque on the source per emitted photon as a function of the parameters η and τ_0.

parameter range. Upon comparing Figs. 4 and 2, it can be seen that for small values of η, the torque exerted on the source is relatively insignificant compared to the torque exerted on the environment. This implies that it is primarily the environment that acquires AM. However, as η increases, this is no longer the case. For $\eta = 0.3$, the torque on the source becomes comparable to the torque on the environment, though with opposite sign, indicating that they acquire opposite AM. It is worth noting that the curve for $\eta = 0.3$ exhibits oscillations. The cause of these oscillations is not yet fully understood, and it is possible that they are the result of an imperfect average over the dipole gas distribution.

The aim of Fig. 5 is to compare the roles of multiple and single scattering. We compare the radiated AM calculated with multiple scattering (MS) and the radiated angular momentum calculated from N single dipole formula:

$$\kappa_{\mathrm{L}}^{\mathrm{SS}} = \sum_{\alpha} \kappa_{\mathrm{L}}(\boldsymbol{R}_\alpha), \tag{23}$$

where $\kappa_{\mathrm{L}}(\boldsymbol{R}_\alpha)$ is the radiated angular momentum in the presence of a single dipole at $\boldsymbol{R}_\alpha$. The single dipole formula

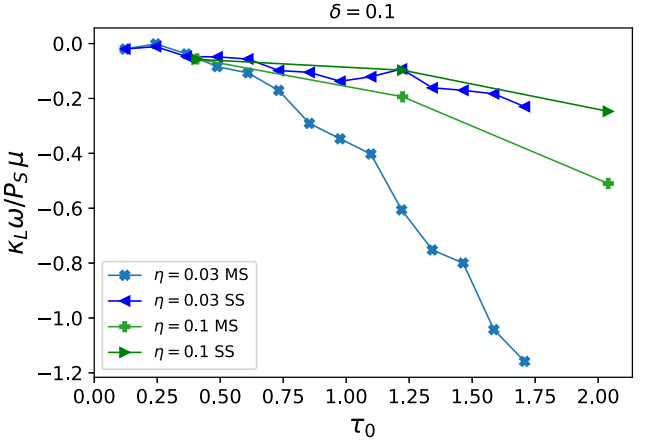

FIG. 5. Effect of multiple scattering on the radiated optical AM. The multiple scattering curves are labeled MS and the single scattering approximation curves are labeled SS.

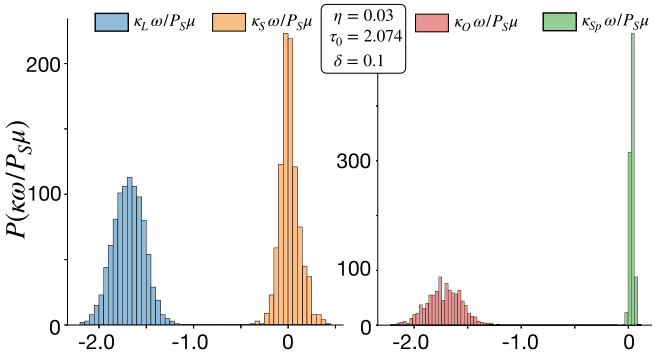

FIG. 6. Left: Distribution of the normalized total leakage $\kappa_{\mathrm{L}}\omega/P_{\mathrm{S}}\mu$ and the normalized torque on the source $\kappa_{\mathrm{S}}\omega/P_{\mathrm{S}}\mu$ for $\eta = 0.03$, optical thickness $\tau_0 = 2.074$ and detuning $\delta = 0.1$. The right figure depicts the distribution of the normalized spin leakage $\kappa_{\mathrm{Sp}}\omega/P_{\mathrm{S}}\mu$ and the normalized $\kappa_{\mathrm{O}}\omega/P_{\mathrm{S}}\mu$ for the same values of η, τ_0, and δ.

by definition neglects any kind of multiple scattering. As expected for $\tau_0 > 1$, the multiple scattering result deviates significantly from the single dipole formula.

The full statistics of the different κ are shown in Fig. 6 for $\eta = 0.03$, $\tau_0 = 2.074$, and $\delta = 0.1$. The standard deviations shown earlier in Fig. 2 correspond to the widths of the probability distribution function for κ_L for the different values of η and τ_0 and are given by the usual formula:

$$\sigma(\tau_0, \eta) = \sqrt{\frac{1}{N}\sum_{i=1}^{N}(\kappa_i - \langle\kappa\rangle)^2}, \tag{24}$$

where N is the number of realizations, κ_i is the value of κ for the realization i, and $\langle\kappa\rangle$ is the mean value of κ over the N realizations. It can be seen from Fig. 2 that as either η or τ increase, the width of the distributions of the radiated AM increases. Thus both the increase in recurrent scattering and the increase in multiple scattering tend to broaden the distributions. The distributions for the spin and orbital AM are seen to be quite different, again revealing the dominant

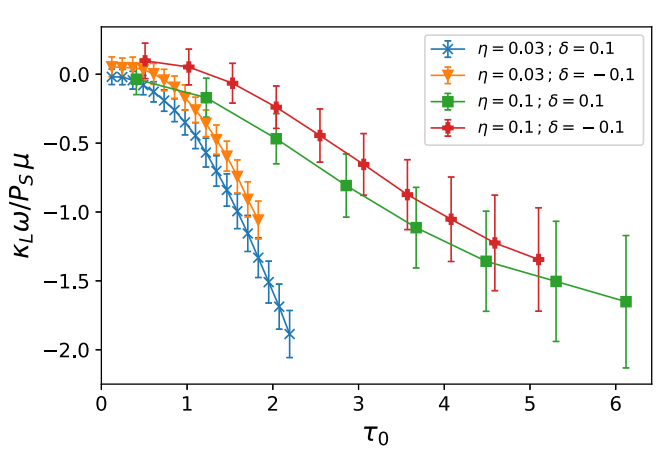

FIG. 7. Impact of opposite detunings on the total AM leakage for the curves $\eta = 0.03$ and $\eta = 0.1$. The bars indicate the standard deviation of the distribution of $\kappa_{\mathrm{L}}\omega/P_{\mathrm{S}}\mu$ values.

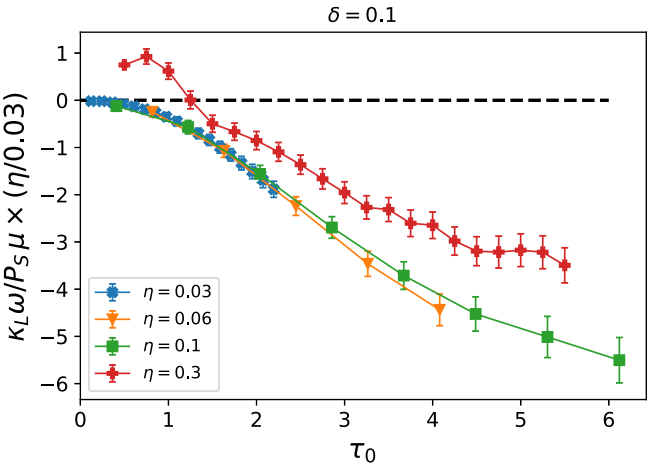

FIG. 8. Single parameter scaling of the normalized angular momentum leak for $\eta = 0.03$, $\eta = 0.06$, $\eta = 0.1$, and $\eta = 0.3$ obtained by multiplying them by $\eta/0.03$. For $\eta = 0.3$, the scaling starts to break down. This figure shows that for values of η up to 0.1, the total radiated angular momentum is proportional to the mean free path ℓ_0 times $f(\tau_0) \sim \tau_0^2$ for $\tau_0 \leqslant 2$.

role of orbital radiated AM. Contrary to κ_O, the average of κ_{sp} is small because it takes both positive and negative values.

In Fig. 7 we show the effect of taking small opposite detunings on the radiated AM for $\eta = 0.03$ and $\eta = 0.1$. For small values of τ_0, the radiated angular momentum has opposite signs for opposite detunings. This is expected from the single dipole formula, proportional to $\mathrm{Im}\, t_0^2$. As τ_0 approaches unity and beyond, this is no longer the case, and the curves for opposite detunings show similar behavior, with only a slight shift with respect to each other. In Fig. 8 we have made an attempt to find a single-parameter scaling of the AM leak. To this end we multiplied all curves by $\eta/0.03$. There is a good agreement for the curves $\eta = 0.06$ and $\eta = 0.1$, but the curve $\eta = 0.3$ clearly deviates. This figure shows that for values of η up to 0.1, the total radiated angular momentum is proportional to the mean free path ℓ_0 for τ_0 constant. When $\eta \sim 1$, the mean free path is no longer given by the ISA formula (22), and the true value of the optical thickness τ is smaller than τ_0.

VI. CONCLUSION AND OUTLOOK

In this paper we have investigated the transfer of angular momentum radiated by an electric dipole source into a magneto-birefringent environment. Two parameters have been considered for this study: η the density of scatterers per cubic of wavelength and τ_0 the optical thickness in the independent scattering approximation. We have shown that for $\eta \ll 1$ the total radiated angular momentum is proportional to τ_0^2 and opposite to the direction of the magnetic field. However, it is observed that as η approaches unity, the τ_0^2 behavior disappears as τ_0 increases. For constant τ_0, the radiated angular momentum is proportional to the mean free path ℓ_0 as long as the density is small enough ($\eta < 0.1$).

The torque on the medium was separated into the torque on the source and the torque on the environment. Previous work [13] showed that the torque on a homogeneous environment vanishes. For small values of η, the torque on the source is negligible and the torque environment dominates. As η increases, the torque on the source increases while the total radiated angular momentum decreases. We conclude that there is more and more transfer of angular momentum from the source directly to the environment. For $\tau_0 \sim 1.25$ and $\eta = 0.3$ we see a special case with no radiated angular momentum at all; thus the torque on the source is fully compensated by the torque on the environment. Finally, the impact of small opposite detunings δ on the total radiated angular momentum is studied.

We have also separated the total radiated angular momentum into spin and orbital components. Surprisingly, the radiated angular momentum turns out to be dominated in most cases by orbital angular momentum.

This work can be extended to consider a magnetic dipole field rather than a uniform magnetic field, without much qualitative difference. This could be relevant for astrophysical phenomena such as angular momentum transport in stars. Future work could also address the role of loss in the environment. Even loss conserves angular momentum, and loss of photons does not necessarily lead to loss of angular momentum leak per emitted photon. A disordered environment with diamagnetic scatterers facilitates the exact numerical study using numerical diagonalization. The clear disadvantage is the weakness of diamagnetism, quantified by the small value for the material parameter μ in this work. It would be interesting to perform full-wave simulations with ferromagnetic disorder, like, e.g., what was done recently to model Anderson localization of light *ab initio* [19], *r*. A real-life experiment of this kind was already proposed in Ref. [10].

ACKNOWLEDGMENTS

This work was funded by the Agence Nationale de la Recherche (Grant No. ANR-20-CE30-0003 LOLITOP). The structure of this text has been improved with the help of DeepL write.

[1] G. B. Rybicki and A. P. Lightman, *Radiative Processes in Astrophysics* (Wiley, Hoboken, NJ, 1991).
[2] See, e.g., M. Bordag, G. Klimchitskaya, U. Mohideen, and V. Mostepanenko, *Advances in the Casimir Effect* (Oxford University Press, Oxford, England, 2009).
[3] P. C. W. Davies, J. Opt. B: Quantum Semiclassical Opt. **7**, S40 (2005).
[4] J. B. Pendry, New J. Phys. **12**, 033028 (2010).
[5] M. R. C. Mahdy, D. Gao, W. Ding, M. Q. Mehmood, M. Nieto-Vesperinas, and Q. Cheng-Wei, arXiv:1509.06971.
[6] A. Dupays, C. Rizzo, D. Bakalov, and G. F. Bignami, Europhys. Lett. **82**, 69002 (2008).
[7] R. G. S. El-Dardiry, S. Faez, and A. Lagendijk, Phys. Rev. A **83**, 031801(R) (2011).
[8] E. M. Purcell, Phys. Rev. **69**, 37 (1946).

[9] L. Landau and E. Lifshitz, *The Classical Theory of Fields* (Pergamon Press, New York, 1975), Sec. 75, p. 193, Problem 2.
[10] B. A. van Tiggelen and G. L. J. A. Rikken, Phys. Rev. Lett. **125**, 133901 (2020).
[11] B. A. van Tiggelen, Opt. Lett. **48**, 41 (2023).
[12] L. D. Barron, *Molecular Light Scattering and Optical Activity* (Cambridge University Press, Cambridge, England, UK, 2004).
[13] B. A. van Tiggelen and S. E. Skipetrov, Phys. Rev. B **103**, 174204 (2021).
[14] R. G. Newton, *Scattering Theory of Waves and Particles,* 2nd ed. (Dover Publications, Mineola, NY, 2013).
[15] L. Landau and E. Lifshitz, *The Classical Theory of Fields* (Pergamon Press, New York, 1975).
[16] B. A. van Tiggelen, R. Maynard, and T. M. Nieuwenhuizen, Phys. Rev. E **53**, 2881 (1996).
[17] C. Cohen-Tannoudji, J. Dupont-Roc, and G. Grynberg, *Photons et Atomes - Introduction à l'éLectrodynamique Quantique* (EDP Sciences, Les Ulis, France, 1987).
[18] L. Dal Negro, *Waves in Complex Media* (Cambridge University Press, Cambridge, England, UK, 2022).
[19] A. Yamilov, S. E. Skipetrov, T. W. Hughes, M. Minkov, Z. Yu, and H. Cao, Nat. Phys. **19**, 1308 (2023).